DOI: 10.1021/ma101975j

Macromolecules
ARTICLE

Single Molecules Probing the Freezing of Polymer Melts: A Molecular Dynamics Study for Various Molecule-Chain Linkages

R. A. L. Vallée,*,† W. Paul,‡ and K. Binder§

†*Centre de Recherche Paul Pascal (CNRS), 115 avenue du docteur Albert Schweitzer, 33600 Pessac, France,* ‡*Institut für Physik, Martin-Luther University, 06099 Halle, Germany, and* §*Institut für Physik, Johannes-Gutenberg University, 55099 Mainz, Germany*

Received August 27, 2010; Revised Manuscript Received November 2, 2010

ABSTRACT: We present molecular dynamics simulations of coarse-grained model systems of a glass-forming polymer matrix containing fluorescent probe molecules. These probe molecules are either dispersed in the matrix or covalently attached to the center or the end of a dilute fraction of the polymer chains. We show that in all cases the translational and rotational relaxation of the probe molecules is a faithful sensor for the glass transition of the matrix as determined from a mode-coupling analysis or Vogel−Fulcher analysis of their α-relaxation behavior. Matrix and dumbbell related relaxation processes show a clear violation of the Stokes−Einstein−Debye laws. In accordance with recent experimental results, the long time behavior of single molecule spectroscopy observables like the linear dichroism is not susceptible to distinguish between center-attached and end-attached fluorophores. However we show that it is different from the behavior of dispersed fluorophores. We also show that the difference between the two attachment forms does show up in the caging regime of the relaxation functions and that this difference increases upon supercooling the melt toward its glass transition.

Introduction

Understanding the mechanisms responsible for the tremendous slowing down of the mobility when approaching the glass transition is one of the most important challenges in modern soft condensed matter physics, both for low-molecular-weight and polymeric materials.[1−5] Rotational motions of both backbone segments and side groups are the principal relaxation mechanisms in amorphous polymers. Such relaxation processes have been studied experimentally in the vicinity of the glass-transition temperature T_g by viscosity,[6] compliance,[6] quasi-elastic neutron scattering,[7] NMR,[8−10] photon correlation spectroscopy,[11,12] dielectric relaxation,[13−15] photobleaching,[16] and second harmonic generation techniques[17,18] to name and cite but a selection of the studies performed. It has been established that above the glass-transition temperature, the α-relaxation is the primary relaxation process for the collective motion of polymer segments.

Because it allows bypassing the ensemble averaging intrinsic to bulk studies, single molecule spectroscopy (SMS) constitutes a powerful tool to assess the dynamics of heterogeneous materials at the nanoscale level.[19−22]

On the one hand, by following the temporal evolution of the fluorescence lifetime of single molecules with quantum yield close to unity, this observable revealed highly sensitive to changes in local density occurring in a polymer matrix.[23−28] Using free volume theories, the lifetime fluctuations were related to hole (free-volume) distributions and allowed the determination of the number of polymer segments involved in a rearrangement cell around the probe molecule as a function of temperature,[23,26] solvent content,[24] and film thickness.[25] On the basis of a microscopic model for the fluctuations of the local field,[27] a clear correlation was established between the fluorescence lifetime distributions measured for single molecules and the local fraction of surrounding holes both in the glassy state and in the supercooled regime for various molecular weight oligo(styrene).[28] Furthermore, fluorescence lifetime trajectories of single probe molecules embedded in a glass-forming PS melt were shown to exhibit strong fluctuations of a hopping character. Using MD simulations targeted to explain these fluctuations,[29] the lifetime fluctuations were correlated with the meta-basin transitions in the potential energy landscape of the polymer matrix, thus providing a new tool for the experimental study of long-standing issues in the physics of the glass transition. Finally, the interaction between the probe molecule and the polymer matrix can also be investigated. The interaction between several conformers of a given fluorophore and poly(styrene) (PS) polymer chains was investigated.[30−32] The existence of different conformations, stabilized owing to favorable interactions with the surrounding polymer matrix, lead to specific spectroscopic responses, i.e., specific fluorescence lifetimes and emission spectra. The type of conformer found in the matrix and its interaction with the surrounding chains governed the local packing of the matrix and thus allowed one to probe the local free volume.

On the other hand, single-molecule rotational imaging also proved to be very powerful in probing the local dynamics of polymers. By using two-dimensional (2D) orientation techniques, the in-plane (of the sample) projection of the transition dipole moment of the single molecule (SM) (the so-called linear dichroism $d(t)$) has been followed in time and its time correlation function $C_d(t)$ has been computed and fitted by a stretched exponential function $f(t) = e^{-(t/\tau)^\beta}$.[33−36] These investigations have allowed to identify static and dynamic heterogeneity in the samples;[37,38] i.e., SMs exhibit τ and β values varying according to (i) their actual position in the matrix and (ii) the time scale at which they are probed, as a result of the presence of different nanoscale environments. Zondervan et al.[39] investigated the rotational motion of perylene diimide in glycerol. Observations of environmental exchanges were very

*To whom correspondence should be addressed. E-mail: vallee@crpp-bordeaux.cnrs.fr.

 Published on Web 12/06/2010

scarce. They assumed that glycerol consists of heterogeneous liquid pockets separated by a network of solid walls. This was supported by rheology measurements at very weak stresses of glycerol and *o*-terphenyl.[40] With 3D orientation techniques, the emission transition dipole moment of a SM has been recorded as a function of time.[41−44] In particular, the distribution of nanoscale barriers to rotational motion has been assessed by means of SM measurements[45] and related to the spatial heterogeneity and nanoscopic α-relaxation dynamics deep within the glassy state. Owing to the high barriers found in the deep glassy state, only few SMs were able to reorient, while somewhat lower barriers could be overcome when increasing the temperature.

However, in all investigations described here above, the local dynamics of the polymers was ascertained through the behavior of single molecules inserted as dopants in the host polymer. Very scarce studies of the motion of the polymer chains themselves have been reported.[46,47] Bowden et al.[46] prepared several polymers with a perylene diimide dye at the end or in the middle of each polymer chain, and the orientation of the labeled segments of polybutadiene (PB) chains in a matrix of poly(methyl methacrylate) (PMMA) was detected using a fluorescence polarization modulation technique. However, the PMMA matrix used in those experiments was glassy and reorientation occurred for only 5% of the dye-labeled polymers. Since the dye was intimately attached to the polymer backbone, the orientation of the dye reflected the motion of the local portion of the polymer chain. The extent to which the dye orientation could be used to infer the overall motion of the entire polymer molecule still has to be elucidated.

It is clearly of interest to further study segmental polymer motion in less rigid environments, such as melts and rubbers. Gravanovich et al.[47] investigated the dynamics of various dye-labeled polymer chains in similar but unlabeled polymer chains in the melt. Their experiments notably allowed for the analysis of the importance of factors such as the position of the dye molecule in the chain, the chemical identity of the dopant and matrix polymers and the pumping intensity on the observed rotational dynamics of the dye. Using autocorrelation analysis of both the total emitted intensity and the orientation angle, a few conclusions were reported: (i) there was no distinguishable difference in the characteristic correlation times between center- and end-positioned dyes; (ii) molecules in the rubbery matrix displayed the longest correlation times while those in the low-viscosity host displayed the shortest times; (iii) the laser illumination intensity had little impact on the intensity autocorrelation decay times, but higher intensity did lead to shorter correlation times in the angle autocorrelation analysis. This seemed to indicate that high intensity provided more thermal energy for the molecules to reorient. The authors[47] further concluded that the dye molecule is quite large compared to the size of a monomer so that the innate motion of the chain might be altered. As such, while the observed motion of the dye molecules might not be representative of unhindered polymer motion, these dyes certainly behave as reporters of the local environment surrounding their position at either the chain end or the chain center. The similar behaviors exhibited for end- and center-labeled dyes on the rather long time scales addressed in the experiments might suggest that differences between the mobilities of chain ends and chain centers had been averaged out on the long time scale, but might still be observable at shorter times. The authors suggested further experiments to examine untethered fluorophores in these polymer melts to compare their behavior to those built into the polymer backbone. By following such parameters as the in-plane dipole moment and the overall brightness of the fluorophore over time and versus temperature can lend insight into dynamic processes that occur within the polymer host.

The aim of our current paper is precisely to shed some light on the dynamical behavior of fluorophores positioned in the center, at the end and simply mixed to polymer chains, to investigate the difference between these behaviors and the bulk relaxation of the polymer itself. For probe molecules dispersed into a glass-forming polymer matrix we have analyzed in detail their ability to faithfully monitor the glass transition of the host matrix. We have shown that the probes record a change in mechanism from rotational diffusion to large angular jumps[48] on approaching the mode-coupling critical temperature of the polymer melt, have analyzed how the coupling between probe and melt depends on the size and the mass of the probe[49] and have shown that the probes are sensitive to chain length effects in the glass transition of the matrix.[50] These studies have employed molecular dynamics simulations of a bead−spring dumbbell dissolved in a bead−spring polymer melt as a coarse-grained model system for probe molecules in a polymer matrix. We are employing the same model here but now attach the probe dumbbell into a polymer chain, either at the end or in the center of the chain.

In the next section, we will explain our simulation model and the way the simulations were performed, and the ensuing section will discuss our results for the translational and rotational dynamics of probes in a polymer matrix, comparing free probes to end-attached and center-attached probes. A final section will then present our conclusions.

Methods

We performed MD simulations of a system containing 48 bead−spring chains of 25 effective monomers. A dumbbell is also inserted in the system to act as a reporter of the behavior of the local environment, mimicking a single molecule as used in single molecule spectroscopy (SMS). The dumbbell has been either inserted as a free dopant (further named free) in the system or covalently linked in the middle (further named center) or at the end (further named end) of one chain of the simulation box, keeping the total number of beads to 25. While our aim is not a chemically realistic modeling of a particular material since we wish to elucidate the generic behavior of polymer melt plus probe molecule systems, the mass of the beads have been chosen to be $m_B = 1$ for the monomers of the chains and $m_A = 2.25$ for the monomers of the dumbbell in order to closely match the experimental conditions[47] for which the probe molecules are always heavier than a dimer in the chains. A cubic simulation volume with periodic boundary conditions is used throughout. The interaction between two beads of type A (probe) or B (monomers) is given by the Lennard-Jones potential

$$U_{LJ}(r_{ij}) = 4\varepsilon\left[\left(\frac{\sigma_{\alpha\beta}}{r_{ij}}\right)^{12} - \left(\frac{\sigma_{\alpha\beta}}{r_{ij}}\right)^{6}\right]$$

where r_{ij} is the distance between beads i, j and $\alpha,\beta \in$ A,B. The LJ diameters used are $\sigma_{AA} = 1.22$, $\sigma_{BB} = 1.0$ (unit of length) and $\sigma_{AB} = 1.11$, while $\varepsilon = 1$ sets the scale of energy (and temperature T, since Boltzmann's constant $k_B = 1$). These potentials are truncated at $r_{cut}^{\alpha\beta} = 2^{7/6}\sigma_{\alpha\beta}$ and shifted so that they are zero at $r_{ij} = r_{cut}^{\alpha\beta}$. Between the beads along the chain, as well as between the beads of the dumbbell, a finitely extendable nonlinear elastic (FENE) potential is used

$$U_F = -\frac{k}{2}R_0^2 \ln\left[1 - \left(\frac{r_{ij}}{R_0}\right)^2\right]$$

with parameters $k = 30$, $R_0 = 1.5$.[51] This model system (without the probe) has been shown to qualitatively reproduce many features of the relaxation of glass-forming polymers.[51−59] In the MD simulations, the equations of motion at constant particle number N, volume V, and energy E are integrated with the velocity Verlet algorithm[60,61] with a time step of 0.002, measuring time in units of $(m_B\sigma_{BB}^2/48\varepsilon)^{1/2}$. All NVE simulations have been performed after equilibrating the system in the NpT ensemble,

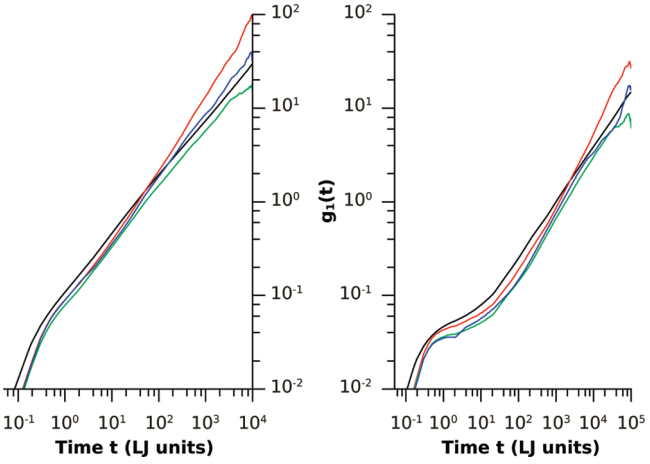

Figure 1. Mean square displacements as a function of time for $T = 0.7$ (left) and $T = 0.5$ (right). The black curves describe $g_1(t)$ for all the monomers of all the chains for the bulk model system. The red, green and blue curves pertain to similar information for the free dumbbell, the dumbbell covalently linked in the center or at the end of one chain, respectively.

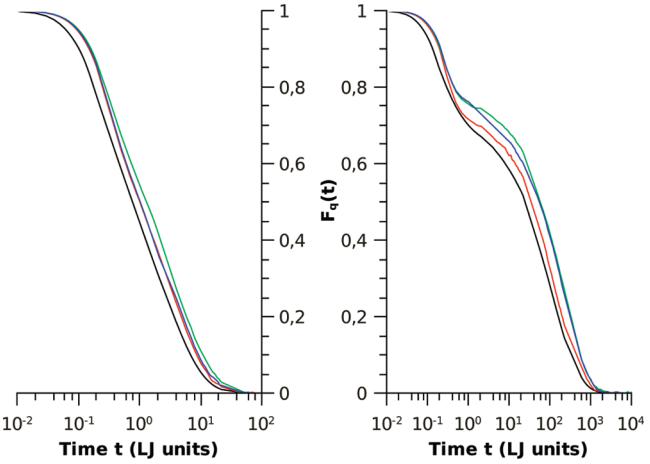

Figure 2. Intermediate dynamic structure factor $F_q(t)$ at the first maximum ($q = 6.9$) of the static structure factor for the NVE simulations performed at temperatures $T = 0.7$ (left) and $T = 0.5$ (right). The black curves describe $F_q(t)$ for the chains in the bulk model system. The red, green, blue curves pertain to similar information for the free dumbbell, the dumbbell covalently linked in the center or at the end of one chain, respectively.

using a Nosé−Hoover thermostat,[61] keeping the average pressure at $p = 1.0$ at all temperatures. These runs lasted up to 5×10^7 MD steps. Ten different configurations were simulated at each temperature ($T = 0.47, 0.48, 0.49, 0.5, 0.55, 0.6, 0.65, 0.7, 1.0, 2.0$), in order to ensure good statistics. Note that the melting temperature of the crystalline phase of this model polymer has been estimated[57] to be $T_m = 0.75$ while the critical temperature T_c of mode coupling theory (where in our model a smooth crossover to activated dynamics occurs) is about $T_c = 0.45$.[50] Thus, our data include equilibrated melts as well as the moderately supercooled regime.

Results

We begin by analyzing the translational motion of the probes and the monomers as observed in the simulation in the mean square displacement of the particles and in simulation and experiment in the incoherent scattering function. The mean square displacements of individual effective monomers is defined as

$$g_1(t) \equiv \frac{1}{M}\sum_{i=1}^{M}\langle[\vec{r}_i(t) - \vec{r}_i(0)]^2\rangle \qquad (1)$$

when we average over all monomers within a polymer chain. The long time behavior of the mean square displacement defines the translational diffusion coefficient, D_t, by

$$g_1(t) = 6D_t t \qquad (2)$$

We obtain the diffusion constant in this work by fitting this linear law to the late time behavior of the mean squared displacement. As we will see in Figure 1, this entails some systematic error because our results for the late time displacement of the dumbbells are susceptible to large statistical fluctuations. For the chain attached dumbbells there is furthermore an extended crossover regime from Rouse-mode dominated to free diffusion behavior and we can not claim in all cases that this crossover is completed within our simulation time window. The incoherent intermediate scattering function, $F_q(t)$, is defined as

$$F_q(t) = \frac{1}{M}\sum_{i=1}^{M}\langle\exp[i\vec{q}\cdot(\vec{r}_i(0) - \vec{r}_i(t))]\rangle \qquad (3)$$

In eq 3, the sum is extended over all M effective monomers in the system, and $\vec{r}_i(t)$ is the position of the i'th monomer at time t, while $\vec{q}$ is the scattering wave vector. Being interested in the slow dynamics associated with the cage effect,[2] it is most useful to choose q such that it roughly corresponds to the position where the static structure factor $S(q)$ of the melt has its peak, which is (for the chosen conditions) $q = 6.9$ (note that in the temperature regime of interest, $S(q)$ changes with temperature only very little. Of course, analogous quantities to eq 1 and eq 3 can be immediately defined for the dumbbell if the simulated system contains one; the only problem then is that, due to the small number $M = 2$ (rather than $M = 1200$), the poor statistics necessitates to carry out multiple runs (as mentioned in the Methods, 10 independent runs were hence performed). In Figure 1 we show results for the mean square displacements for all monomers g_1, of all chains and for the dumbbells included in the melt for two temperatures. The higher temperature, $T = 0.7$ displayed on the left shows the typical melt behavior in the polymer displacements. After an initial inertia dominated period, lasting until $t \simeq 0.5$, one observes, in the monomer displacement, a crossover to a subdiffusive, Rouse mode dominated regime, and at long times another crossover to the free diffusion limit, from which we read of the translational diffusion coefficient at that temperature. At the lower temperature, $T = 0.5$, depicted on the right, a plateau regime is clearly visible in the monomer displacement extending about one decade in time. This regime of caged dynamics is indicative of the approach to the glass transition in the supercooled melt. When we analyze the motion of the dumbbell as an indicator for the matrix glass transition, we observe that it mirrors the matrix behavior irrespective of whether it is free (red curves), center-attached (green curves), or end-attached (blue curves). The free dumbbell is not following the late stages of the Rouse mode dominated dynamics and crosses over to free diffusion at an earlier time than the chains. Both chain-attached dumbbells of course have to participate in the Rouse mode dynamics of the chains. While at the higher temperature the end-attached dumbbell seems to be slightly faster than the center-attached one for displacements larger than one monomer diameter, there is no discernible difference between these displacements at the lower temperature. However, we have to keep in mind the limited statistical accuracy we can obtain with one dissolved dumbbell for the long-time behavior of correlation functions, even when we average over 10 independent runs.

When we now look at the incoherent intermediate scattering function shown in Figure 2, we can observe the same built-up of a two-step relaxation behavior upon approach of the glass transition

as discussed for the mean square displacements. At both temperatures, all dumbbell scattering functions relax more slowly than the monomer one. At the higher temperature there is an observable difference between the free dumbbell and the end-attached dumbbell on the one side and the center-attached dumbbell on the other side, which relaxes more slowly than the other two for times around the typical relaxation time (time to decay to $1/e$) which is about 5. We can see in Figure 1 that at these times the spheres have moved over roughly 20% of their diameter and for these time scales Figure 1 also displays a slightly slower motion of the center-attached dumbbell than of the end-attached one, although this feature, is hardly visible on the logarithmic scale of Figure 1.

Looking at the lower temperature, we see interesting differences developing in the mobilities of the dumbbells. In the inertia regime, all dumbbells move in the same way and similarly to the monomers of the chains. The inertial regimes end at around $t \simeq 0.5$. The extent of motion, however, is very different for the different situations. The scattering function of the monomers decays faster and to the largest extent through the inertial and vibrational motion. Next comes the free dumbbell which relaxes more slowly but to almost the same extent. The slower motion can be understood by a larger resistance that the dumbbell experiences compared to two bonded monomers due to the increased diameter of the spheres making up the dumbbell. The inertial relaxation of the dumbbell is damped on the same time scale as for the surrounding matrix, and the extent of its relaxation is limited by that of the matrix. The chain-attached dumbbells share the inertia time scale with the free dumbbell, but the extent of the inertial relaxation is much smaller, that is, they are experiencing about the same amount of spatial constraint, i.e., caging. The end-attached dumbbell, however, is able to break out of the cage earlier than the center-attached dumbbell, so its relaxation is faster in the β-regime and early α-regime in the nomenclature of mode-coupling theory. In the late alpha regime, i.e., for the final 50% of the relaxation the relaxation functions for both dumbbell types agree again, however. This indicates that this regime is determined by Rouse mode contributions affecting all parts of the chain in a similar way.

To investigate the behavior of the end-attached and center-attached dumbbells in this plateau regime in more detail, we plot in Figure 3 their mean square displacements as well as the corresponding incoherent scattering functions at two slightly lower temperatures, $T = 0.49$ and $T = 0.47$. At $T = 0.49$, we observe the behavior discussed above for $T = 0.5$: the end-attached dumbbell breaks out of the plateau regime earlier than the center-attached dumbbell. At $T = 0.47$, however, closer to the mode-coupling temperature, this behavior has changed and the behavior of both dumbbells is not longer distinguishable. This indicates that at the onset of the caging ($T = 0.5$ and $T = 0.49$) chain connectivity plays a stronger role than deeper in the caging regime ($T = 0.47$) where packing effects dominate.

We turn now to the rotational relaxation of the matrix and the probes which is accessible through SMS techniques. Defining $\vec{u}(t)$ as a unit vector along the axis connecting the positions of the two particles in the dumbbell at time t, one defines orientational time correlation functions in terms of

$$\cos(\theta(t)) = \vec{u}(t)\cdot\vec{u}(0) \tag{4}$$

via the Legendre polynomials $P_\ell(\cos\theta)$ as

$$C_\ell(t) \equiv P_\ell(\cos\theta(t)) \tag{5}$$

and corresponding relaxation times

$$\tau_\ell = \int_0^\infty C_\ell(t)\,\mathrm{d}t$$

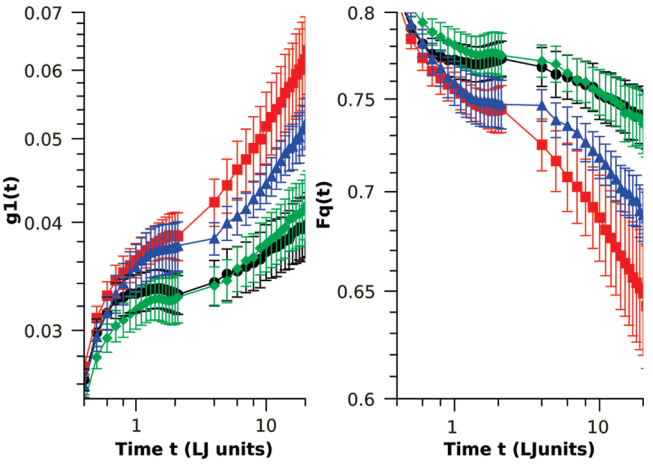

Figure 3. Mean squared displacement (left side) and incoherent scattering function (right side) of end-attached dumbells (red squares are for $T = 0.49$ and black circles are for $T = 0.47$) and center-attached dumbbells (blue triangles are for $T = 0.49$ and green diamonds are for $T = 0.47$). Error bars are from a Jacknife procedure of the simulation trajectory.

Here we have determined also analogous data for the orientational correlations of bonds in the polymer chain, which can be defined in the same way by averaging the data over either the last bonds or all bonds except the last ones in all polymer chains, to compare to the two bonding situations of the dumbbells. In many single molecule spectroscopy (SMS) studies, emphasis is put on the measurement of the linear dichroism trajectories, $d(t)$. In terms of the single molecule emission intensity along two mutually perpendicular polarization direction I_p and I_s, $d(t)$ is defined as

$$d(t) = (I_p - I_s)/(I_p + I_s) \tag{6}$$

In simulations, an equivalent quantity can be defined as[62]

$$d(t) = (7/8)[(\vec{e}_1\cdot\vec{u})^2 - (\vec{e}_2\cdot\vec{u})^2] \tag{7}$$

where $\vec{e}_1$ and $\vec{e}_2$ are unit vectors along the two in-plane orthogonal polarization directions of the system, and $\vec{u}$ is the unit vector along the dumbbell axis, as before.

As an example we display the second Legendre polynomial autocorrelation function of bonds and dumbbells in Figure 4 for the same two temperatures studied in Figure 1 and Figure 2. For the bond-correlations, obviously the orientation of the less constraint bonds at chain ends decorrelates faster than in the center of the chain. For the dumbbell we observe for both temperatures a stronger decorrelation due to the short time inertial regime than for the bonds. All dumbbell correlation functions are, however, more strongly stretched in the β-relaxation regime than the bond correlation functions so that their asymptotic decay occurs on a longer time scale. Here the free dumbbell shows the fastest decorrelation, followed by the end-attached dumbbell, and the center-attached dumbbell has the largest relaxation time. In the late α-relaxation regime, however, the dumbbell correlation functions and the bond-correlation functions are more or less parallel shifted with respect to each other, indicating that in this time regime it is the relaxation behavior of the matrix which determines also the relaxation of the dumbbells, irrespective of whether they are free or chain-attached.

For all relaxation functions discussed above, we can define a measure for the α-relation time τ_x of the various observables (incoherent scattering function $F_q(t)$: $x = q$, linear dichroism $C_d(t)$: $x = d$ and second order Legendre polynomials $C_2(t)$: $x = 2$ autocorrelation functions by the condition

$$(F/C)_x(t = \tau_x) = 0.3 \tag{8}$$

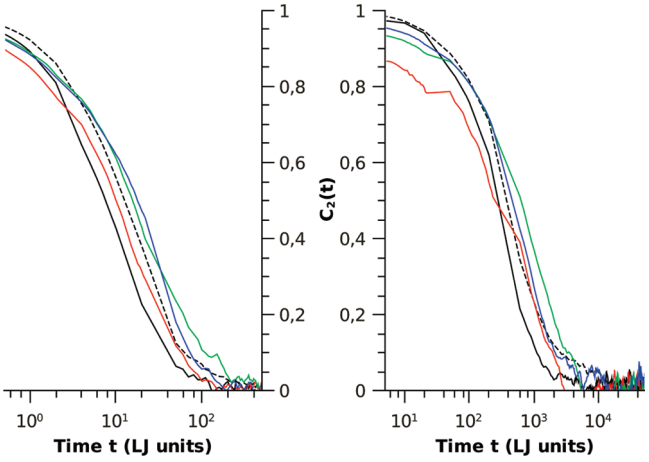

Figure 4. Second order Legendre polynomials autocorrelation functions as a function of time for $T = 0.7$ (left) and $T = 0.5$ (right). The solid (dashed) black curves describe $C_2(t)$ for the bonds at the end (in the center, respectively). The red, green, and blue curves pertain to similar information for the free dumbbell, the dumbbell covalently linked in the center or at the end of one chain.

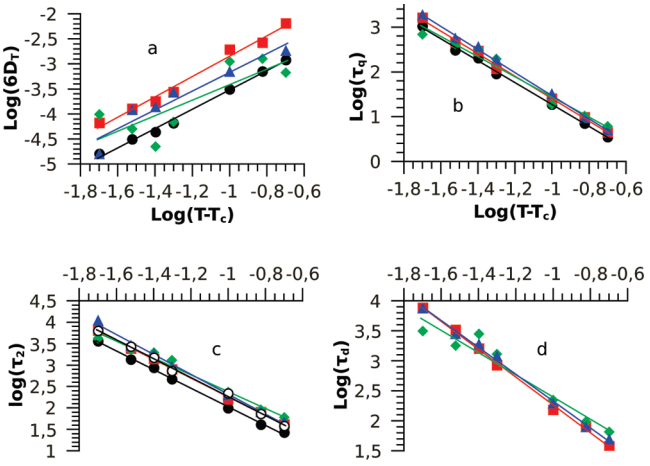

Figure 5. Log−log plots of the translational diffusion coefficients D_t (a) and of the relaxation times τ_q (b), τ_2 (c), and τ_d (d) for the pure polymer system (black circles), the free dumbbell (red squares), the dumbbell covalently linked in the center (green diamonds) or at the end (blue triangles) of one chain. All relaxation times have been determined empirically by the requirement $(F/C)_x(\tau_x) = 0.3$. The parameters γ obtained from the fits to a power law (see text) are given in Table 1. There are no linear dichroism data (d) for the bulk model system because of the lack of characterization technique in this case. In the case of the orientational second order correlation function (c) for the bulk model system, we did differentiate the function where only monomers at the end (filled black circles) of the chains were taken into account from the one where all the monomers except the ones at the end (open black circles) of the chains were taken.

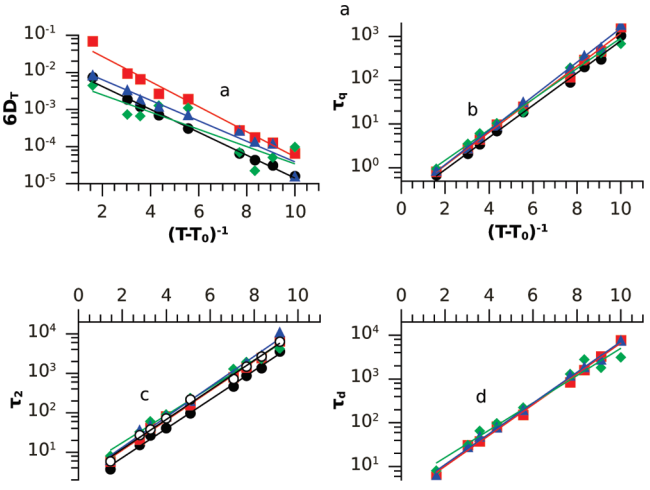

Figure 6. Same as Figure 5 but in a Vogel−Fulcher format.The values of the Vogel temperature T_0 and of the fragility parameter B/T_0 are presented in Table 2.

For these α-relaxation times and for the translational diffusion coefficient several predictions for their temperature dependence exist in the literature, the most prominent ones being the mode coupling law[2]

$$D_t \propto (T/T_c - 1)^{\gamma} \tag{9}$$

or

$$\tau_x \propto (T/T_c - 1)^{-\gamma} \tag{10}$$

and the Vogel−Fulcher relation[63]

$$\tau = \tau_0 \exp[B/(T - T_0)] \tag{11}$$

Here τ_0 is a prefactor setting the high-temperature time scale, B is some effective activation energy, and T_0 the Vogel−Fulcher temperature. Comparing Figure 5 and Figure 6 we can see that both the MCT law and the Vogel−Fulcher law provide a reasonable description of our data in the simulated temperature range, when we keep the MCT critical temperature T_c or the Vogel−Fulcher temperature T_0 fixed to their known values for the pure polymer melt system. The essential parameters of these fits are the exponent γ for the MCT power law (see Table 1) and a measure for the fragility B/T_0 for the Vogel−Fulcher law (see Table 2). For the α-relaxation exponent γ we observe a grouping of the fit values with significant scatter between the fits. However, the fit values for the diffusion coefficient are smallest on average, followed by the values for the orientation correlation functions which are similar and, finally, the γ values for the incoherent scattering function are largest. Such a difference in γ value has been observed before comparing relaxation functions involving different length scales,[54] e.g., incoherent scattering functions at different q-values. For our correlation functions this signifies that the orientation correlations are susceptible to larger scale motions than the incoherent scattering function at the wave vector shown. Addressing the scatter between the different fit values for the different dumbbells, we can plot relaxation functions as functions of time in units of the α-relaxation time (Figure 7).

Then we observe that the curves for the incoherent scattering function for all dumbbells and for the temperatures $T = 0.47$, 0.48, 0.49, 0.5 basically scale on top of each other in the late β, early α regime, and the same is true for the orientation correlation functions C_2 and C_d. Performing an analysis of these scaled functions with an extended von Schweidler law

$$H(t) = f - h\left(\frac{t}{\tau_\alpha}\right)^{b} + hB\left(\frac{t}{\tau_\alpha}\right)^{2b} \tag{12}$$

$H(t)$ standing for either $F_q(t)$ or $C_2(t)$ or $C_d(t)$, yields nonergodicity parameters of $f = 0.73$ for the incoherent scattering and $f = 0.87$ for the orientation correlation functions, as well as von Schweidler exponents of $b = 0.57$ and $b = 0.66$. These in turn yield $\gamma = 2.48$ for the scattering and $\gamma = 2.26$ for the orientation correlations employing the exponent relations of MCT. These values are well compatible with the exponents found from free fitting of the temperature dependence of the α-relaxation times in Figure 5. The variation in values reported in Table 1 is therefore attributable to the statistical uncertainty of our data and not

Table 1. γ Parameters Obtained by Fitting the MCT Law to the α Relaxation Times τ_q, τ_2, and τ_d and to the Translational Diffusion Coefficients D_t for the Pure Polymer System, the Free Dumbbell, the Dumbbell Covalently Linked in the Center or at the End of One Chain[a]

	γ			
	D_t	τ_q	τ_2	τ_d
bulk	1.93	2.44	2.21 (c), 2.17 (e)	
free	2.03	2.51	2.18	2.32
center	1.55	2.25	1.96	1.85
end	1.87	2.58	2.32	2.24

[a] The results of the fits were obtained by fixing the critical temperature $T_C = 0.45$.

Table 2. B/T_0 Parameters Obtained by Fitting the Vogel−Fulcher Law to the α Relaxation Times τ_q, τ_2, and τ_d and to the Translational Diffusion Coefficients D_t for the Pure Polymer System, the Free Dumbbell, the Dumbbell Covalently Linked in the Center or at the End of One Chain[a]

	B/T_0			
	D_t	τ_q	τ_2	τ_d
bulk	1.92	2.28	2.13 (c), 2.10 (e)	
free	2.10	2.35	2.14	2.19
center	1.45	2.17	1.99	1.94
end	1.72	2.42	2.19	2.18

[a] The results of the fits were obtained by fixing the Vogel temperature to $T_0 = 0.37$.

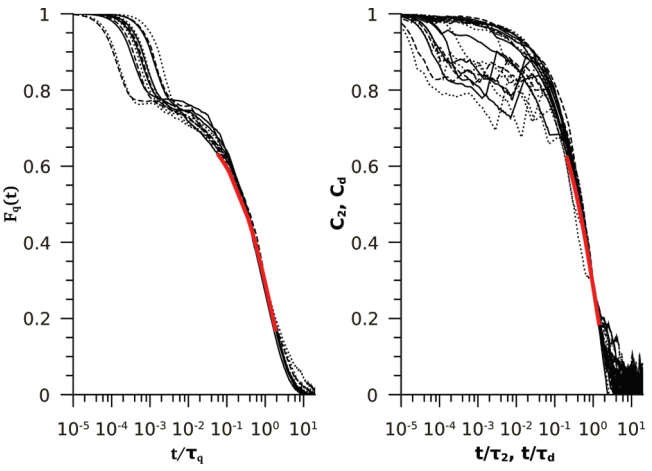

Figure 7. Incoherent scattering function (left side) and orientation correlation functions (right side) plotted vs time scaled by the respective α-relaxation time. The plots contain data for all three types of dumbbell attachment and the temperatures $T = 0.47, 0.48, 0.49, 0.5$. The red line (light gray line) is an extended von Schweidler fit to the scaling regime in these master plots (see text).

indicative of a difference in behavior between the differently attached dumbbells. However, the difference in γ value between the incoherent scattering data and the orientation correlation functions is significant and in agreement with what was discussed before.[54]

For the fragility parameter from the Vogel−Fulcher law no clear trends are discernible. Concerning the flexibility of the Vogel−Fulcher law as a phenomenological fitting function and the limited available temperature range from our simulations, the differences between the quoted B/T_0 values probably just reflect the uncertainty of the fitting procedure.

Figure 5 and Figure 6 confirm again our earlier conclusion that the dynamics of the dumbbells, whether dispersed freely in the polymer matrix or attached covalently to a chain is a faithful

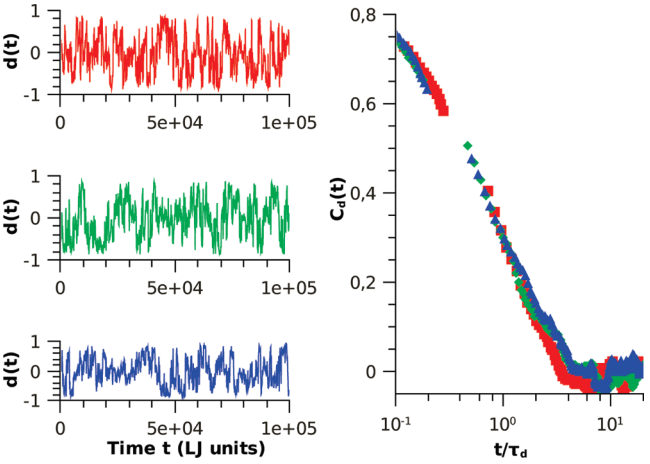

Figure 8. Left: Linear dichroism $d(t)$ trajectories of a free dumbbell (red curve), a dumbbell covalently linked in the center (green curve) or at the end (blue curve) of one chain in a model system at a temperature of $T = 0.5$. Right: Corresponding (red squares, green diamonds, and blue triangles, respectively) orientational time correlation functions $C_d(t)$ versus time scaled by the α-relaxation time τ_d of the linear dichroism.

probe of the glass transition in the matrix. Keeping the critical temperatures fixed in our fits was just necessitated by the statistical scatter, especially for the single dumbbell data. Averaging experimentally over a sufficiently large ensemble of individually measured SMS data will, however, be necessary to determine critical parameters for the MCT law or the Vogel−Fulcher law with sufficient accuracy. Independent of whether we choose to analyze correlation functions in terms of the MCT or the Vogel−Fulcher law, we can plot them versus scaled time, scaling by the respective estimate for the α-relaxation time determined as described above. Figure 8 shows such a plot for the linear dichroism which is the quantity of central interest in SMS experiments. On the left side of the figure we display single time traces of the dichroism signal as obtained for the free, center-attached or end-attached dumbbell (from top to bottom). All three look very similar, with perhaps a subtle difference between the center-attached and end-attached dumbbell on the one hand and the free dumbbell on the other hand. The latter one seems to have a fluctuation pattern somewhat more homogeneous in time than the former two. This subtle difference is also observable in the dichroism time-correlation function shown on the right side of the figure. The curves for the chain-attached dumbbells are more stretched than the one for the free dumbbell, although the observed effect is rather small. One may speculate that this hints at a larger dynamic heterogeneity for the chain-attached dumbbells increasing at lower temperature, especially going below the mode coupling T_c and approaching the calorimetric glass transition temperature T_g. After all, it is this temperature regime where experiments typically show an increase of dynamic heterogeneity.[37]

Dynamic heterogeneity is also at the origin of the breakdown of the Stokes−Einstein and Stokes−Einstein−Debye laws in glass forming materials, leading, e.g., to a power law relation between translational diffusion coefficient and correlation time

$$D_t \propto (\tau_q/T)^{-\xi_t} \tag{13}$$

We have documented this breakdown before[49,50] for our model system and showed that it occurs for the pure polymer and the dumbbell within the matrix as a probe of the matrix glass transition in the same way. In Figure 9 we show a double logarithmic plot of the translational diffusion coefficient as a function of relaxation time over temperature. The exponents for the plotted fit lines are given in Table 3. The exponent values for the pure polymer and the free dumbbell have been reported earlier.[50] They

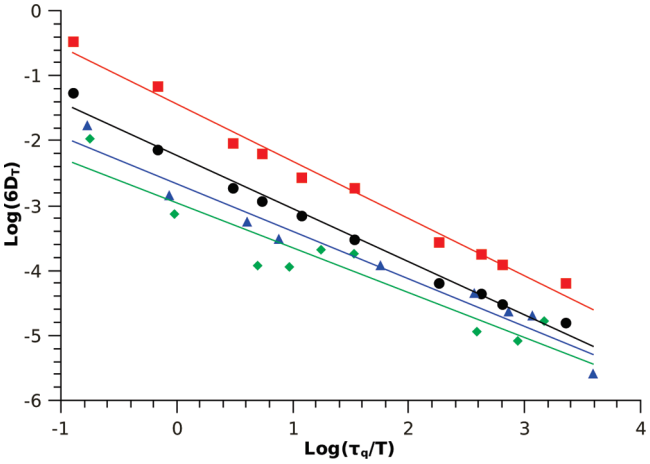

Figure 9. Power law fits of translational diffusivities D_t as a function of $\tau_q/T(q = 6.9)$: $D_t \approx (\tau_q/T)^{-\xi_t}$ for the bulk (black circles) or the dumbbell either free (red squares) or covalently linked in the center (green diamonds) or at the end (blue triangles) of one chain. Results for the ξ_t exponent are given in Table 3.

Table 3. ξ_t Parameters Obtained by Fitting the Fractional Functional Forms (SE Relation Modified by ξ_t) to the Relaxation Times τ_q for Either the Pure Polymer System, the Free Dumbbell, the Dumbbell Covalently Linked in the Center or at the End of One Chain

$$D_t \propto \left(\frac{\tau_q}{T}\right)^{-\xi_t}$$

	ξ_t
bulk	0.82
free	0.88
center	0.69
end	0.73

are about 10% larger than the values found for the chain-attached dumbbells.

Conclusions

We have performed molecular dynamics simulations of a model system for a glass forming polymer melt into which fluorescent molecules are embedded. Our simulations mimic recent experiments where a fluorophore is either dispersed into the host matrix or where it is covalently bound into the center or at the end of a dilute fraction of chains in the melt. These fluorophores are studied by single molecule spectroscopy techniques and are employed as probes of the glass transition of the melt. Addressing single molecules offers the possibility to study spatial and dynamic heterogeneity in the melt on a single molecule level.

While the measurement of temperature dependence of different translational and rotational autocorrelation functions for the embedded fluorophores in principle allows to determine various characteristic temperatures of the glass forming matrix such as the mode-coupling T_c or the divergence temperature T_0 of the Vogel−Fulcher law, reducing the statistical scatter in such measurements to a sufficient degree to allow for an accurate determination of these temperatures requires a significant experimental effort in averaging over a large sample of independent molecules.

We had shown in earlier studies that a fluorescent molecule dispersed into the polymer melt can be a faithful probe of the glass transition in the host matrix. We show here that this remains true for chain-attached probes as well. Our findings for the dichroism autocorrelation functions agree with the experimental observation in ref 47 that they show no discernible difference for different attachments in the chain. However, we would suggest that experimentally such a comparison should be made to the autocorrelation of dispersed dumbbells which should show a less stretched decay, i.e., smaller dynamic heterogeneity.

While there are no discernible differences in the long-time relaxation behavior of the chain-attached probes (late α-relaxation times), there seem to be subtle differences on the time scale on which the caging between neighboring chains in the melt occurs. These time scales could not be probed in the SMS experiments so far.[46,47] End-attached and center-attached dumbbell are experiencing an equal localization scale in the caging regime, but the end-attached dumbbell breaks out of this caging at a smaller time scale than the center-attached one. We have shown this behavior to occur upon approaching the mode-coupling T_c but experimentally it might be still better observable at temperatures closer to T_g which are not accessible in our simulations. On the one hand, the corresponding time scales then are larger and on the other hand, our results indicate that the difference between the relaxation behavior of the two types of chain-attached dumbbells increases upon cooling.

Acknowledgment. R.A.L.V. thanks the Fonds voor Wetenschappelijk Onderzoek (FWO) Vlaanderen for a postdoctoral fellowship. Partial support from Sonderforschungsbereich 625/A3 of the German National Science Foundation and the EU network of excellence SOFTCOMP is also acknowledged.

References and Notes

(1) Jäckle, J. *Rep. Prog. Phys.* **1986**, *49*, 171.
(2) Götze, W.; Sjögren, L. *Rep. Prog. Phys.* **1992**, *55*, 241.
(3) See: Debenedetti, P. G. *Metastable Liquids*; Princeton Univ. Press: Princeton, NJ, 1997.
(4) See: Donth, E.-W. *The Glass Transition. Relaxation Dynamics in Liquids and Disordered Materials*; Springer: Berlin, 2001.
(5) See: Binder, K.; Kob, W. *Glassy Materials and Disordered solids. An Introduction to their Statistical Mechanics*; World Scientific: Singapore, 2005.
(6) Plazek, D. J. *J. Phys. Chem.* **1965**, *69*, 3480.
(7) Kanaya, T.; Kawaguchi, T.; Kaji, K. *J. Chem. Phys.* **1996**, *104*, 3841.
(8) Pschorn, U.; Rössler, E.; Kaufmann, S.; Sillescu, H.; Spiess, H. W. *MacromoleculEs* **1991**, *24*, 398.
(9) Kuebler, S. C.; Heuer, A.; Spiess, H. W. *Phys. Rev. E* **1997**, *56*, 741.
(10) He, Y.; Lutz, T. R.; Ediger, M. D.; Ayyagari, C.; Bedrov, D.; Smith, G. D. *Macromolecules* **2004**, *37*, 5032.
(11) Lee, H.; Jamieson, A. M.; Simha, R. *Macromolecules* **1979**, *12*, 329.
(12) Patterson, G. D.; Lindsey, C. P. *J. Chem. Phys.* **1979**, *70*, 643.
(13) Saito, S.; Nakajima, T. *J. Appl. Polym. Sci.* **1959**, *4*, 93.
(14) Fukao, K.; Miyamoto, Y. *J. Non-Cryst. Solids* **1994**, *172*−*174*, 365.
(15) León, C.; Ngai, K. L.; Roland, C. M. *J. Chem. Phys.* **1999**, *110*, 11585.
(16) Inoue, T.; Cicerone, M. T.; Ediger, M. D. *Macromolecules* **1995**, *28*, 3425.
(17) Dhinojwala, A.; Wong, G. K.; Torkelson, J. M. *J. Chem. Phys.* **1994**, *100*, 6046.
(18) Hall, D. B.; Deppe, D. D.; Hamilton, K. E.; Dhinojwala, A.; Torkelson, J. M. *J. Non-Cryst. Solids* **1998**, *235*−*237*, 48.
(19) Moerner, W. E.; Orrit, M. *Science* **1999**, *283*, 1670.
(20) Xie, X. S.; Trautman, J. K. *Annu. Rev. Phys. Chem.* **1998**, *49*, 441.
(21) Kulzer, F.; Orrit, M. *Annu. Rev. Phys. Chem.* **2004**, *55*, 585.
(22) Vallée, R. A. L.; Cotlet, M.; Hofkens, J.; De Schryver, F. C.; Müllen, K. *Macromolecules* **2003**, *36*, 7752.
(23) Vallée, R. A. L.; Tomczak, N.; Kuipers, L.; Vancso, G. J.; van Hulst, N. F. *Phys. Rev. Lett.* **2003**, *91*, 038301.
(24) Vallée, R. A. L.; Tomczak, N.; Kuipers, L.; Vancso, G. J.; van Hulst, N. F. *Chem. Phys. Lett.* **2004**, *384*, 5.
(25) Tomczak, N.; Vallée, R. A. L.; van Dijk, E. M. H. P.; Kuipers, L.; van Hulst, N. F.; Vancso, G. J. *J. Am. Chem. Soc.* **2004**, *126*, 4748.
(26) Vallée, R. A. L.; Tomczak, N.; Vancso, G. J.; Kuipers, L.; van Hulst, N. F. *J. Chem. Phys.* **2005**, *122*, 114704.
(27) Vallée, R. A. L.; Van der Auweraer, M.; De Schryver, F. C.; Beljonne, D.; Orrit, M. *ChemPhysChem* **2005**, *6*, 81.
(28) Vallée, R. A. L.; Baruah, M.; Hofkens, J.; De Schryver, F. C.; Boens, N.; Van der Auweraer, M.; Beljonne, D. *J. Chem. Phys.* **2007**, *126*, 184902.

(29) Vallée, R. A. L.; Van der Auweraer, M.; Paul, W.; Binder, K. *Phys. Rev. Lett.* **2006**, *97*, 217801.
(30) Vallée, R. A. L.; Marsal, P.; Braeken, E.; Habuchi, S.; De Schryver, F. C.; Van der Auweraer, M.; Beljonne, D.; Hofkens, J. *J. Am. Chem. Soc.* **2005**, *127*, 12011.
(31) Braeken, E.; Marsal, P.; Vandendriessche, A.; Smet, M.; Dehaen, W.; Vallée, R. A. L.; Beljonne, D.; Van der Auweraer, M. *Chem. Phys. Lett.* **2009**, *472*, 48.
(32) Braeken, E.; De Cremer, G.; Marsal, P.; Pépe, G.; Müllen, K.; Vallée, R. A. L. *J. Am. Chem. Soc.* **2009**, *131*, 12201.
(33) Deschenes, L. A.; Vanden Bout, D. A. *J. Phys. Chem. B* **2002**, *106*, 11438.
(34) Tomczak, N.; Vallée, R. A. L.; van Dijk, E. M. H. P.; García-Parajó, M.; Kuipers, L.; van Hulst, N. F.; Vancso, G. J. *Eur. Polym. J.* **2004**, *40*, 1001.
(35) Schob, A.; Cichos, F.; Schuster, J.; von Borczyskowski, C. *Eur. Polym. J.* **2004**, *40*, 1019.
(36) Mei, E.; Tang, J.; Vanderkooi, J. M.; Hochstrasser, R. M. *J. Am. Chem. Soc.* **2003**, *125*, 2730.
(37) Ediger, M. D. *Annu. Rev. Phys. Chem.* **2000**, *51*, 99.
(38) Richert, R. *J. Phys.: Condens. Matter* **2002**, *4*, R703.
(39) Zondervan, R.; Kulzer, F.; Berkhout, G. C. G.; Orrit, M. *Proc. Natl. Acad. Sci. U.S.A.* **2007**, *104*, 12628.
(40) Zondervan, R.; Xia, T.; van der Meer, H.; Storm, C.; Kulzer, F.; van Saarloos, W.; Orrit, M. *Proc. Natl. Acad. Sci. U.S.A.* **2008**, *105*, 4993.
(41) Dickson, R. M.; Norris, D. J.; Moerner, W. E. *Phys. Rev. Lett.* **1998**, *81*, 5322.
(42) Sick, B.; Hecht, B.; Novotny, L. *Phys. Rev. Lett.* **2000**, *85*, 4482.
(43) Lieb, A.; Zavislan, J. M.; Novotny, L. *J. Opt. Soc. Am. B* **2004**, *21*, 1210.
(44) Böhmer, M.; Enderlein, J. *J. Opt. Soc. Am. B* **2000**, *20*, 554.
(45) Bartko, A. P.; Xu, K.; Dickson, R. M. *Phys. Rev. Lett.* **2002**, *89*, 026101.
(46) Bowden, N. B.; Willets, K. A.; Moerner, W. E.; Waymouth, R. M. *Macromolecules* **2002**, *35*, 8122.
(47) Gavranovich, G. T.; Csihony, S.; Bowden, N. B.; Hawker, C. J.; Waymouth, R. M.; Moerner, W. E.; Fuller, G. G. *Macromolecules* **2006**, *39*, 8121.
(48) Vallée, R. A. L.; Paul, W.; Binder, K. *Europhys. Lett.* **2007**, *79*, 46001.
(49) Vallée, R. A. L.; Paul, W.; Binder, K. *J. Chem. Phys.* **2007**, *127*, 154903.
(50) Vallée, R. A. L.; Paul, W.; Binder, K. *J. Chem. Phys.* **2010**, *132*, 034901.
(51) Bennemann, C.; Paul, W.; Binder, K.; Dünweg, B. *Phys. Rev. E* **1998**, *57*, 843.
(52) Bennemann, C.; Baschnagel, J.; Paul, W.; Binder, K. *Comput. Theor. Polym. Sci.* **1999**, *9*, 217.
(53) Bennemann, C.; Baschnagel, J.; Paul, W. *Eur. Phys. J B* **1999**, *10*, 123.
(54) Bennemann, C.; Paul, W.; Baschnagel, J.; Binder, K. *J. Phys.: Cond. Matter* **1999**, *11*, 2179.
(55) Baschnagel, J.; Bennemann, C.; Paul, W.; Binder, K. *J. Phys.: Condens. Matter* **2000**, *12*, 6365.
(56) Aichele, M.; Baschnagel, J. *Eur. Phys. J. E* **2001**, *5*, 229. ibid 245.
(57) Buchholz, J.; Paul, W.; Varnik, F.; Binder, K. *J. Chem. Phys.* **2002**, *117*, 7364.
(58) Baschnagel, J.; Varnik, F. *J. Phys.: Condens. Matter* **2005**, *17*, R851.
(59) Paul, W. In *Reviews in Computational Chemistry*; Wiley: New York, 2007, Vol. *25*, p 1.
(60) The software package OCTA (http://octa.jp) was used.
(61) Binder, K., Ciccotti, G., Eds. *Monte Carlo and Molecular Dynamics of Condensed Matter*; Societa Italiana di Fisica: Bologna, 1996.
(62) Gelin, M. F.; Kosov, D. S. *J. Chem. Phys.* **2006**, *125*, 054708.
(63) Vogel, H. *Phys. Z.* **1921**, *22*, 645. Fulcher, G. S. *J. Am. Ceram. Soc.* **1925**, *8*, 339.